APH Inhibitors that Reverse Aminoglycoside Resistance in Enterococcus casseliflavus

Elise Kaplan, Laurent Chaloin, Jean-françois Guichou, Kévin Berrou, Rahila Rahimova, Gilles Labesse, Corinne Lionne

ChemMedChem

Research Article
doi.org/10.1002/cmdc.202400842

Chemistry Europe
European Chemical Societies Publishing

www.chemmedchem.org

APH Inhibitors that Reverse Aminoglycoside Resistance in *Enterococcus casseliflavus*

Elise Kaplan,*[a, c] Laurent Chaloin,[a] Jean-François Guichou,[b] Kévin Berrou,[a] Rahila Rahimova,[b, d] Gilles Labesse,[b] and Corinne Lionne*[a, b, e]

Aminoglycoside-phosphotransferases (APHs) are a class of bacterial enzymes that mediate acquired resistance to aminoglycoside antibiotics. Here we report the identification of small molecules counteracting aminoglycoside resistance in *Enterococcus casseliflavus*. Molecular dynamics simulations were performed to identify an allosteric pocket in three APH enzymes belonging to 3′ and 2″ subfamilies in which we then screened, *in silico*, 12,000 small molecules. From a subset of only 14 high-scored molecules tested *in vitro*, we identified a compound, named here **EK3**, able to non-competitively inhibit the APH(2″)-IVa, an enzyme mediating clinical gentamicin resistance. Structure-activity relationship (SAR) exploration of this hit compound allowed us to identify a molecule with improved enzymatic inhibition. By measuring bacterial sensitivity, we found that the three best compounds in this series restored bactericidal activity of various aminoglycosides, including gentamicin, without exhibiting toxicity to HeLa cells. This work not only provides a basis to fight aminoglycoside resistance but also highlights a proof-of-concept for the search of allosteric modulators by using *in silico* methods.

Introduction

Aminoglycosides such as gentamicin and streptomycin are broad-spectrum polycationic antibiotics often used to treat severe bacterial infections due to a variety of aerobic Gram-negative and Gram-positive microorganisms.[1] They promote mistranslation or inhibition of the translation by targeting the A-site of the 30S ribosomal subunit, leading to the lethal accumulation of aberrant proteins.[2,3] The rapid bactericidal activity,[4] prolonged post-antibiotic effect,[5] and synergism of aminoglycosides with cell-wall synthesis inhibitors including ampicillin and vancomycin[6,7] makes them particularly effective antimicrobial tools. They are prescribed, for example, for the treatment of endocarditis, urinary tract infections or septicemia. However, their use in clinics has become limited by the emergence of bacterial resistance.

Among the different mechanisms of antibiotic resistance, clinical aminoglycoside resistance is predominantly supported by the active alteration of the antibiotic by aminoglycoside-modifying enzymes (AMEs).[8,9] Once inside the bacterial cell, the drug is enzymatically modified which compromises its efficient binding to the ribosomal target.[10] Genes encoding AMEs are often located on transposable genetic elements associated with other antibiotic resistance determinants, encoding β-lactamases or different AMEs, which promotes the rapid diffusion of antibiotic resistance within bacterial populations.

Currently more than a hundred AMEs have been identified which belong to the evolutionary distinct families of aminoglycoside acetyl-, nucleotidyl-, or phosphotransferases.[8,11] One bi-functional enzyme carries both acetylation and phosphorylation activities.[12,13] Each AME family is further divided into subfamilies, designated by the position of aminoglycoside modification, followed by a Roman numeral and a letter indicating substrate specificities and genetic variabilities respectively.[1] Aminoglycoside phosphotransferases, APHs, catalyze the covalent addition of phosphate groups on aminoglycoside hydroxyl substituents at positions 4, 6, 9, 3′, 2″, 3″ or 7″.[8] APH enzymes use ATP and/or GTP as phosphate donor.

They share a structurally similar nucleotide-binding site with eukaryotic protein kinases.[14] Several efforts have been made to stop aminoglycoside deactivation by designing antibiotics more resistant to enzymatic modification[15–18] or by targeting the nucleotide pocket with inhibitors of protein kinases.[19–21] However, the intrinsically large aminoglycoside versatility of AMEs and the potential cross-reactivity with essential eukaryotic pathways constitute the major limitations for therapeutic

[a] E. Kaplan, L. Chaloin, K. Berrou, C. Lionne
Institut de Recherche en Infectiologie de Montpellier – IRIM, University of Montpellier, CNRS UMR 9004, 1919 route de Mende, 34293 Montpellier cedex 5, France
E-mail: elise.kaplan@cnrs.fr
corinne.lionne@cnrs.fr

[b] J.-F. Guichou, R. Rahimova, G. Labesse, C. Lionne
Centre de Biologie Structurale – CBS, University of Montpellier, CNRS UMR 5048, INSERM U 1054, 29 rue de Navacelles, 34090 Montpellier, France

[c] E. Kaplan
Current address: University of Lyon, CNRS, UMR5086, Molecular Microbiology and Structural Biochemistry, IBCP, 7 Passage du Vercors, 69367 Lyon, France

[d] R. Rahimova
Current address: University of Grenoble Alpes, CEA, CNRS, IBS, Metalloproteins Unit, 71 avenue des Martyrs, CS 10090, 38000 Grenoble, France

[e] C. Lionne
Current address: University of Montpellier, CNRS UMR 5048, INSERM U 1054, CBS, 29 rue de Navacelles, 34090 Montpellier, France

Supporting information for this article is available on the WWW under https://doi.org/10.1002/cmdc.202400842

development of APH inhibitors. Another strategy would be to take advantage of the presence of distinct allosteric sites in the protein, in order to identify small molecules able to block protein dynamics, often essential to its function. In addition, this type of allosteric inhibitor is likely to result in non-competitive inhibition, which has the advantage of being independent of cellular substrate levels and should provide an unprecedented level of specificity. The feasibility of such approach by using allosteric modulators of APHs has been already explored by us[22] and others.[23]

Here, we present a strategy which combines molecular dynamics (MD) simulations, *in silico* screening with enzymatic and antibacterial assays to identify allosteric inhibitors of APHs. From a small subset of molecules tested *in vitro*, we identified a hit compound that reduces enzymatic phosphorylation of aminoglycosides. Optimization of this initial hit led to small molecules able to counteract aminoglycoside resistance in bacteria. This study not only provides a basis to fight aminoglycoside resistance, but may also serve as a template for the development of combined chemotherapies to overcome bacterial resistance and antibiotic obsolescence in a clinical context.

Results and Discussion

Molecular Dynamics Simulations Reveal Potential Allosteric Sites

A visual inspection of the 3D-structures of all APHs indicated potential binding sites near substrate locations. The idea was to find a cavity outside of both substrate binding pockets, that could be targeted by small molecules to block or perturb the protein dynamics. Indeed, conformational flexibility is essential for an efficient catalytic activity. To this end, we performed molecular dynamics (MD) simulations to identify dynamic pockets using three APH enzymes belonging to 3′ and 2″ subfamilies. These APHs represent more than half of the identified APHs and include clinically important members. We selected the APH(3′)-IIIa for its broad spectrum towards 4,6-disubstituted aminoglycosides,[24,25] the APH(2″)-IIa which has been identified in Gram-positive and Gram-negative bacteria[26,27] and the enterococcal APH(2″)-IVa which confers a high level of resistance to gentamicin,[28] one of the most commonly used aminoglycosides in clinics. All three proteins have been well-characterized structurally, and numerous crystal structures are available.[20,25,29–31]

MD simulations of 200 ns were carried out on APH(3′)-IIIa (PDB ID 1J7L), APH(2″)-IIa (4DCA, formerly 3R70) and APH(2″)-IVa (4DBX) structures after removal of bound ligands. The resulting 2,000 frames extracted from the trajectories were analyzed to detect dynamic cavities within the three APHs. As expected, this analysis confirms the presence of the substrate binding pockets but also identified a cavity present in the three APHs, and located behind the nucleotide-binding site (Figures 1A–C). For each protein, we calculated the volume of this cavity all along the simulation. We observed significant volume variations, with 3–4-fold difference between the most open and closed conformations, with a fluctuation of the pocket volume of APH(2″)-IIa ranging from 300–1,100 Å^3 (Figure 1D). Therefore, this cavity can be used to screen small molecules to block protein dynamics and trap the enzyme in a conformational state, making it less efficient.

APH Inhibitor Identified by *in silico* and *in vitro* Screenings

Pre-steady state studies evidenced that the product release (departure of ADP and/or aminoglycoside 3′-phosphate) is the rate-limiting step of the reaction catalyzed by APH(3′)-Ia and APH(3′)-IIa.[32,33] Similarly, by examining the transient kinetics of APH(3′)-IIIa and APH(2″)-IVa, we found similar results and showed that the ADP release constitutes the rate-limiting step of aminoglycoside phosphorylation,[34,35] leading us to consider this property as shared among APH(3′) and APH(2″). An ADP-containing complex is therefore the longest-lived reaction intermediate and constitutes consequently a pertinent target for the discovery of novel, effective and allosteric APH inhibitors.

We performed *in silico* ensemble screening based on the three ADP-bound APH structures and the target cavity identified by analysis of our initial MD simulations. The APH(2″)-IVa·ADP complex was not available at that time, so we generated it from the apo structure (4DBX) guided by the ADP-bound APH(2″)-IIa (4DCA). Commercially available molecules from the ZINC database[36,37] were filtered according to Lipinski's rules of five. Initial screening revealed that the APH(2″)-IVa displayed much lower docking scores than the other two APH proteins. To overcome this disadvantage, a normal modes analysis was performed on the APH(2″)-IVa and a more open conformation of the protein was selected for the docking. We docked into the ensemble of three APH·ADP structures a total of 12,000 filtered small synthetic molecules using GOLD software.[38] For each protein-ligand conformation, the program ranks the small molecules according to a scoring fitness function (GoldScore) which takes into account factors such as protein-ligand hydrogen-bonding and van der Waals energies.[39] We selected a subset of 14 high-scored molecules, hereafter named **EK1**–**EK14**, based on the mean of their predicted binding affinities for all three APHs. The highest docking scores for each small molecule are depicted in Figure 2A and listed in Table S1 with their 2D structures shown in Figure 2B. Some compounds, such as **EK2** or **EK8**, presented similar docking scores for the three proteins while others had very different scores. With the exception of **EK11** and **EK12**, no particular structural consensus was found between the compounds.

The 14 top hit molecules were purchased. Among them, six compounds (**EK1**, **EK8**, **EK9**, **EK11**, **EK12** and **EK14**) presented solubility issues which prevented further testing. The potential of the eight remaining molecules to inhibit aminoglycoside modification *in vitro* was subsequently examined on purified APH proteins using the rapid ADP/NADH coupled-system as previously described.[24] To detect low to mid-level inhibition, EK compounds were screened at a relatively high concentration

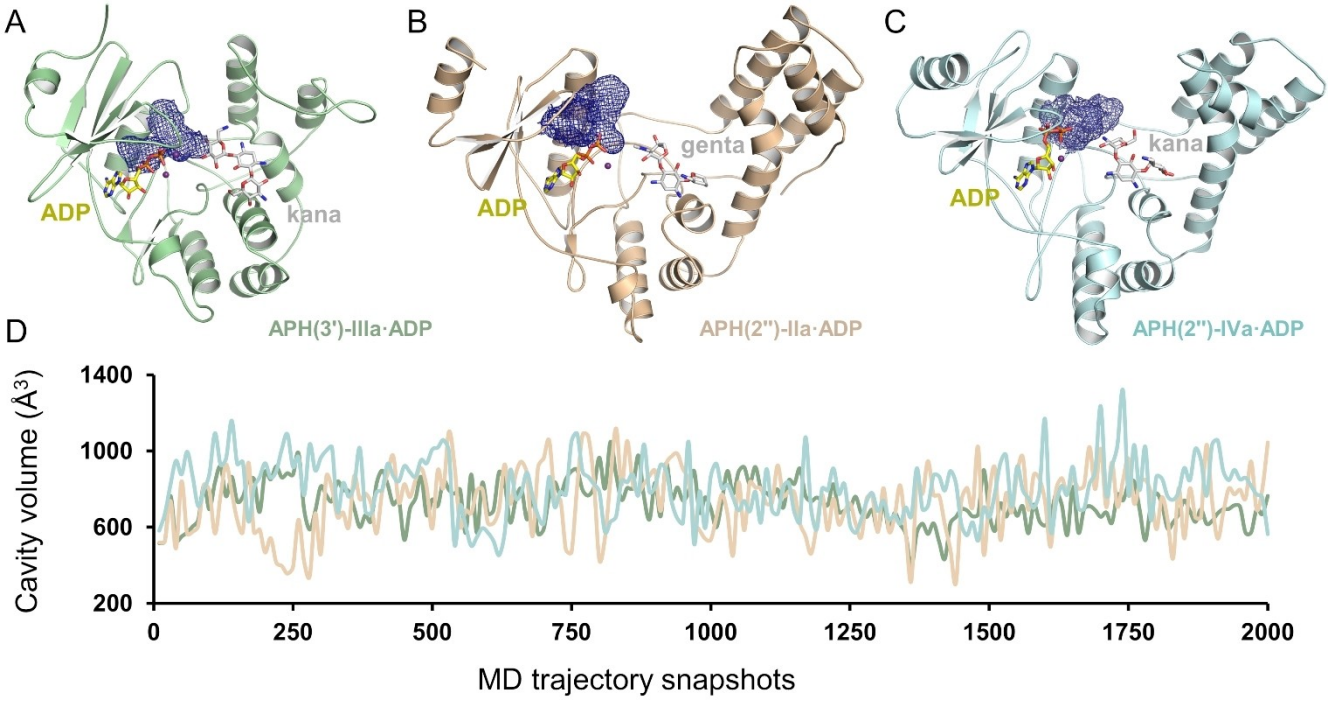

Figure 1. Selection of a target cavity for *in silico* screening of allosteric inhibitors. Crystal structures are (A) APH(3′)-IIIa (1J7L), (B) APH(2″)-IIa (4DCA, superseding 3R70) and (C) APH(2″)-IVa (4DBX). The nucleotides, magnesium ions and aminoglycosides are respectively represented in yellow sticks, purple spheres and grey sticks. In (C), MgADP derives from 4DCA aligned to 4DBX. Aminoglycosides correspond to kanamycin A from 1L8T in (A), gentamicin C1a from 3HAM in (B) and kanamycin A from 4DFB in (C). (D) Distribution of the volume cavity during the MD simulations for APH(3′)-IIIa (green), APH(2″)-IIa (salmon) and APH(2″)-IVa (blue). For clarity, snapshots are shown at 0.1 ns intervals. The first 200 MD snapshots for the three proteins and the corresponding cavities are shown in Movie S1.

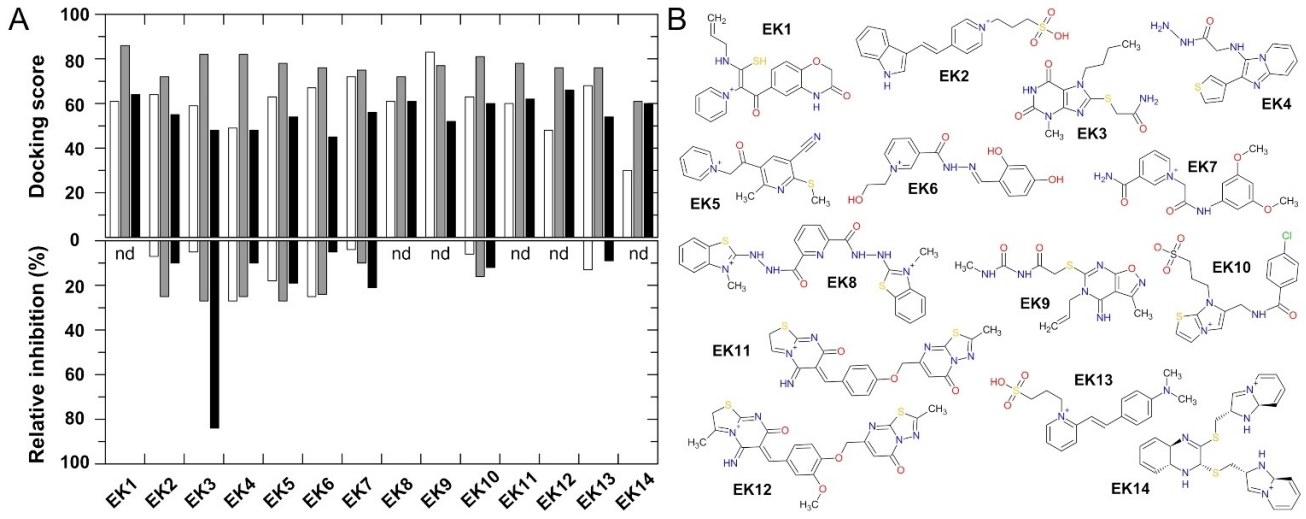

Figure 2. Docking scores and enzymatic APH inhibition of selected EK molecules. (A) Upper panel: *in silico* screening scores on APH(3′)-IIIa (white), APH(2″)-IIa (grey) and APH(2″)-IVa (black) for the 14 selected EK compounds. Lower panel: relative inhibitions of the enzymatic activities by EK compounds. Steady-state rate constants (k_{ss}) were measured using the ADP/NADH coupled assay with final concentrations of 0.5 μM APH enzyme, 100 μM kanamycin A, 350 μM ATP and 500 μM EK compounds, before normalizing the activities to vehicle values. nd (no data) indicates compound solubility issues preventing testing. (B) Corresponding 2D structures of EK molecules. ZINC numbers, docking scores and enzymatic relative activities are fully listed in Table S1.

(500 μM). As shown in Figure 2A, compound **EK3** resulted in low to moderate inhibition of APH(3′)-IIIa and APH(2″)-IIa, but reduced APH(2″)-IVa-mediated kanamycin A modification by over 80%. To further appreciate the basis for this dramatic reduction, we performed biochemical characterization of this hit compound to kinetically define the mechanism of APH inhibition and evaluate its potential toxic effects *in cellulo*.

EK3 is a Non-Competitive Inhibitor of APH(2″)-IVa

Uncharged at physiological pH, **EK3** is a small molecule (311 Da) structurally related to methylxanthine molecules such as caffeine and theophylline. **EK3** is characterized by the presence of a methyl-sulfanyl acetamide group and a 4-carbon aliphatic chain on the imidazole moiety. The compound has a partition coefficient, clogP, of 0.14, and possesses three hydrogen-bond donors and eight acceptors, according to ZINC12.[37] To our knowledge, no patent, nor known or predicted activity has been described for this molecule. However, it has been already selected from another virtual screening and tested *in vitro* against the human S-adenosylmethionine decarboxylase, but did not demonstrate sufficient activity.[40]

We probed the APH inhibition mode of **EK3** by a direct steady-state kinetics measurement using the quench-flow method combined with HPLC nucleotide detection.[35,41] To this end, steady-state rate constants of the reaction were measured at different concentrations of **EK3** and substrates. To determine the mode of inhibition with ATP or kanamycin A, the concentration of the parametric substrate was fixed, close to its respective K_m value, as previously determined.[35,42] Double reciprocal plots revealed non-competitive inhibition of APH(2″)-IVa towards both ATP and kanamycin A substrates with inhibition constants, K_i, of 20 ± 1 and 23 ± 1 μM respectively (Figure 3A and B).

EK3 Hit Optimization

To optimize inhibition potency and to bring structural insights on substituents favorable for potent inhibition, we then performed structure-activity relationship experiments. In the ZINC database and using the Tanimoto index classification,[43] more than 3,000 compounds have a 70% or greater structural identity to **EK3**. We filtered these analogues using the following criteria: equal or greater aqueous solubility compared to **EK3**, low molecular weight (150–600 Da) and commercial availability. The resulting library was then docked into the APH(2″)-IVa·ADP structure using the same parameters as previously set for ensemble docking on the three APHs. Analysis of the docking revealed that 28 molecules scored better than **EK3**, including 5 pairs of enantiomer molecules. We acquired 10 of them based on their similarity with the hit compound and decided to select only one molecule by enantiomer pair. We further included 9 compounds that were less well-ranked but presented interesting features such as a shorter and/or branched aliphatic chain, increased rigidity or small substituent variations. Their docking scores are listed in Table S2. Although its expected solubility is lower than that of the hit compound, **EK3–11** was also selected because it is the acetyl version of **EK3**. All analogues share the same core scaffold (monomethyl-xanthine) with variations along the R_1, R_2 and R_3 positions (Figure 4A). We experimentally probed the APH(2″)-IVa activity with our portfolio of 20 analogues using the direct quench-flow method. As shown in Figure 4B, we observed a general trend of molecules having shorter motifs (<4-carbon chain) in R_2 to be less effective, suggesting that R_2 substituents play a major role in the protein interaction.

This is exemplified by **EK3–13** and **EK3–6** where an additional methyl on R_2, leading to **EK3–17** and **EK3**, increases inhibition by 1.8 and 2.5-fold respectively. Interestingly, **EK3–20** which has a benzene ring at R_2 still reduced APH activity by 40%, suggesting that bulkier R_2 motifs do not prevent enzyme binding. This is confirmed by its high docking score (Figure S2).

At 20 μM, **EK3** reduces APH activity by 50%. A similar or greater effect was recorded with the two analogues **EK3–17** and **EK3–18**, which respectively displayed 50 and 70% inhibition. The two molecules only differ from each other in R_1 where the presence of an acetyl for **EK3–18** lead to a larger inhibition than an amide. However, this does not stand as a general rule (see **EK3** and **EK3–11**). We further characterized **EK3–17** and **EK3–18** and determined their inhibition profile by direct, steady-state kinetics. As for **EK3**, we found that the two analogues display a non-competitive inhibition with respect to both substrates (Figure 5). The inhibition constants for **EK3–17** and **EK3** are comparable, confirming the equivalent activity described previously, while **EK3–18** presented a two-fold smaller K_i with respect to ATP (10 ± 1 μM) and a similar K_i with respect to the aminoglycoside.

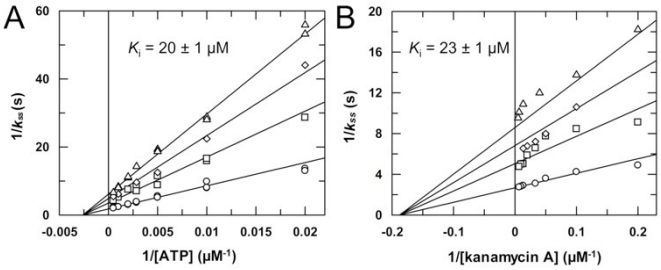

Figure 3. Mode of inhibition of APH(2″)-IVa by EK3. Lineweaver-Burk representation of the non-competitive inhibition profiles of **EK3** with respect to (A) ATP or (B) kanamycin A. Initial concentrations in the reaction mixtures were 0.5 μM APH(2″)-IVa, 20 μM kanamycin A, 50–2000 μM ATP in (A) or 5–200 μM kanamycin A and 400 μM ATP in (B), and 0 (circles), 20 (squares), 35 (diamonds) or 50 (triangles) μM **EK3**. The values of the inhibition constants, K_i, are indicated. Raw data and global fittings according to other modes of inhibition are shown in Figure S1.

Binding Mode of EK3 and Analogues to the APH(2″)-IVa Remains Puzzling

The non-competitive mode of the inhibition of **EK3** compounds is consistent with the initial cavity targeted in our docking studies. Despite numerous trials of co-crystallization, we could not confirm the inhibitor binding site, possibly due to the relatively poor solubility of **EK3** molecules in the crystallization drops and/or the presence of DMSO solvent. However, we determined a crystal structure at 2.40 Å after soaking a crystal of apo APH(2″)-IVa with **EK3–18**, the most potent inhibitor. X-ray data and refinement statistics are given in Table S3. The crystal belongs to space group $P12_11$ and contained two proteins per asymmetric unit. Comparison of the structures of apo APH(2″)-IVa soaked or not with **EK3–18** shows a conforma-

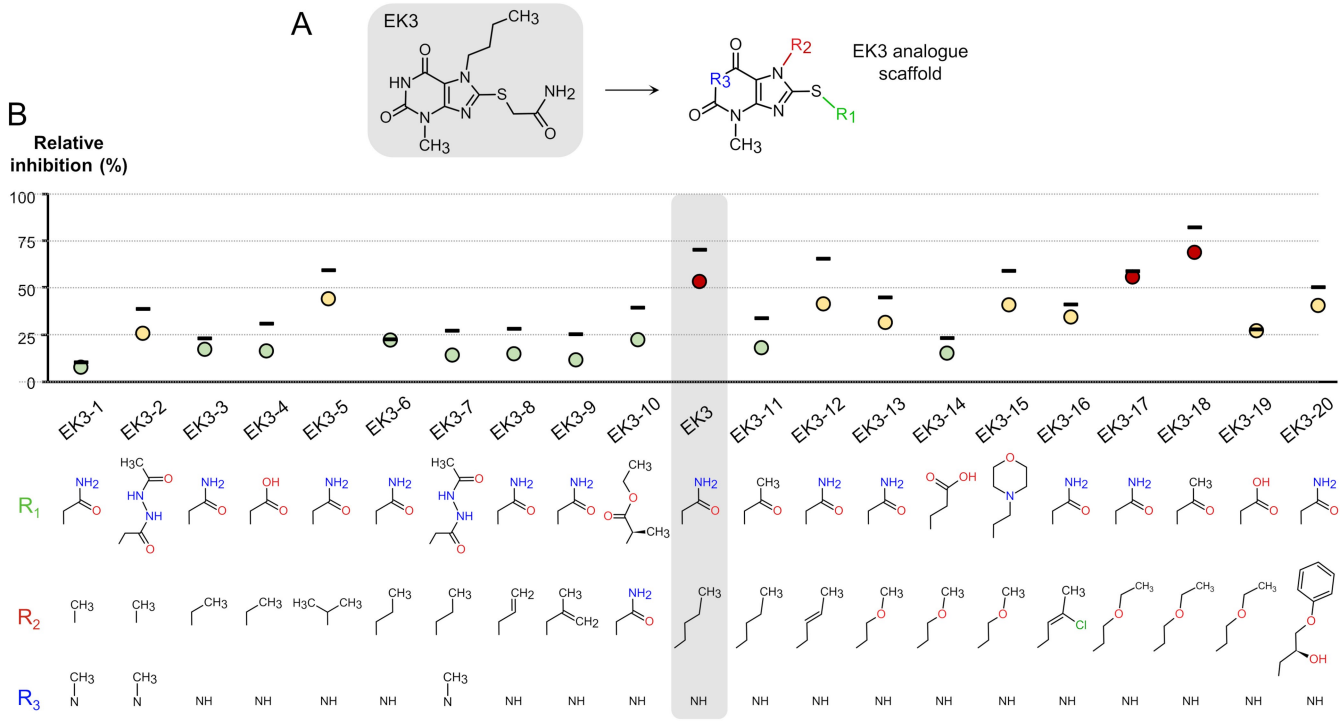

Figure 4. Structure-activity optimization of EK3 for APH(2″)-IVa inhibition. (A) 2D view of **EK3** and the pharmacologic scaffold shared by the 20 purchased analogues, indicating the locations R_1, R_2 and R_3 of structural variations, as further detailed in (B). (B) Relative inhibition of APH(2″)-IVa by **EK3** and 20 analogues. For each molecule, motifs present in R_1, R_2 and R_3 are shown and analogues are organized, left to right, by the increasing length and/or complexity of R_2. Position of **EK3** is marked with a grey frame as in (A). Colored circles depict the level of inhibition: high (more than 50%, red), medium (between 25 and 50%, yellow) or weak (less than 25%, green). Values correspond to the average of two independent repetitions with the upper limit of standard deviation indicated as a horizontal line. Final concentrations were 0.5 μM APH, 20 μM kanamycin A, 400 μM ATP and 20 μM **EK3** and analogue compounds.

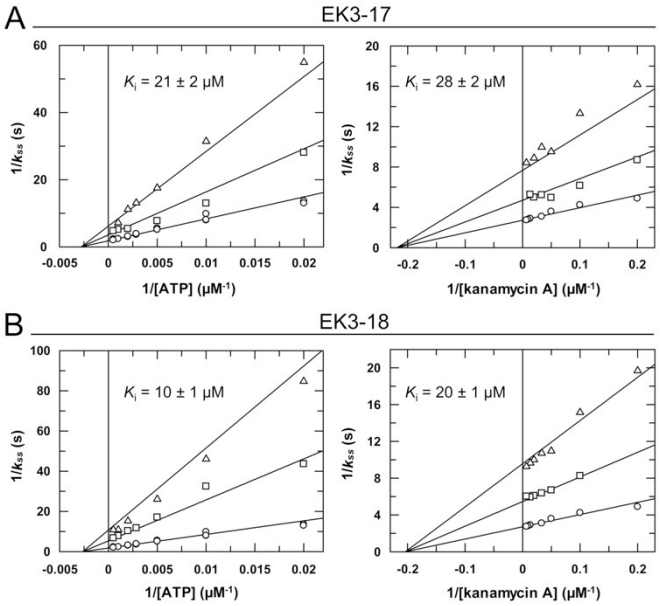

Figure 5. Modes of inhibition of APH(2″)-IVa by EK3–17 and EK3–18 compounds. Lineweaver-Burk representations of the non-competitive inhibition profiles of **EK3–17** (A) and **EK3–18** (B) with respect to ATP (left) and kanamycin A (right). Values of inhibition constants, K_i, are indicated. Final concentrations were as in Figure 3 with 0 (circles), 20 (squares), or 50 (triangles) μM **EK3** analogues. Raw data and global fittings with different modes of inhibition are shown in Figure S2.

tional change in the C-terminal domain of the protein (Figure 6A, Movie S2) where helices α9 and α10 are pushed forward by approximately 6–8 Å. A similar movement was observed in one structure of apo APH (form II), possibly due to dehydration.[44] The latter crystal had a lower solvent content than the other apo structures obtained (form I and III). However, solvent content here was close to 50% and such conformational change was not observed with crystals soaked with just DMSO, nor in other APH(2″)-IVa complex structures (Figure 6B–C), while a similar motion could be obtained on a structure after soaking a crystal with **EK3** (data not shown). Yet, no electron density could be attributed to **EK3–18** in the structure determined here, but we cannot exclude that the conformational change observed here is induced by the presence of the **EK3–18** inhibitor. Further characterizations will be needed to clarify the binding mode of **EK3** inhibitors.

EK3-Based Inhibitors Reverse Aminoglycoside Resistance in APH(2″)-IVa-Producing *Enterococcus Casseliflavus*

To assess the effect of **EK3**-based inhibitors on the bacterial susceptibility to aminoglycosides, we selected an aminoglycoside-resistant *Enterococcus casseliflavus* isolate expressing *aph(2″)-IVa* (CIP 111947, ATCC 700668) from the Pasteur Institute, Paris. Genomic and plasmid DNA of the strain were extracted and used as templates for detection of *aph* genes. We

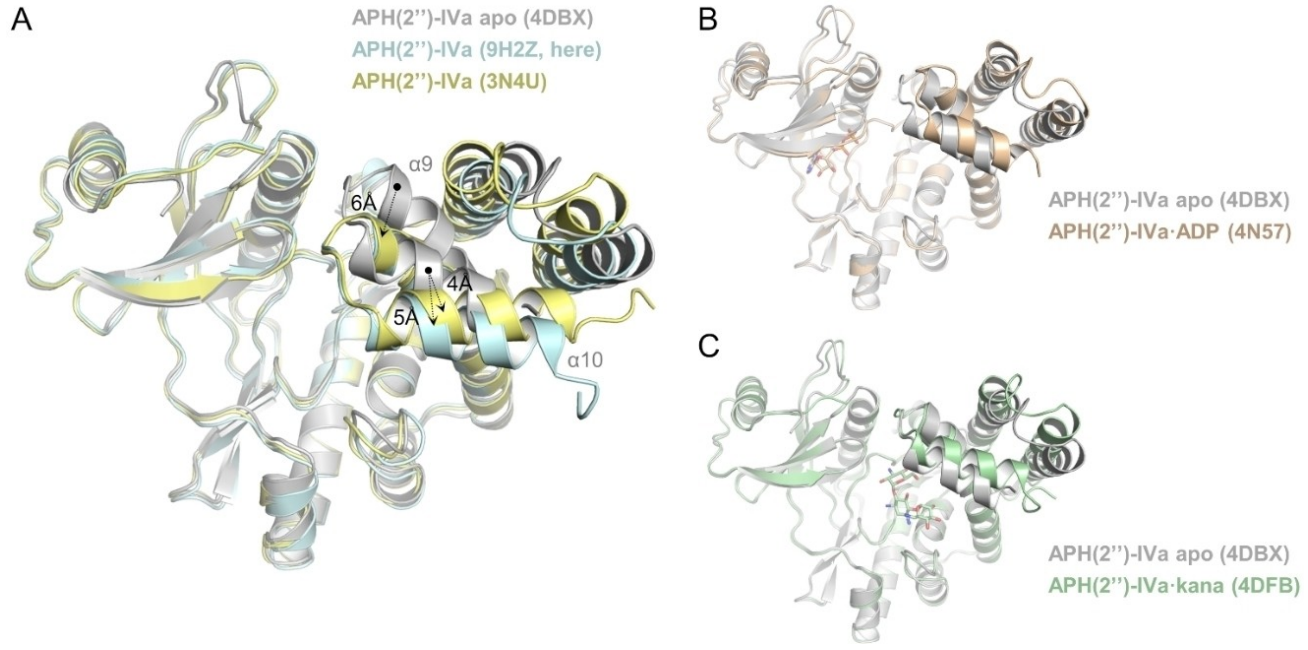

Figure 6. Conformational change of the C-terminal domain of the protein. Overlay of crystal structures of APH(2″)-IVa in apo form (grey, 4DBX) and (A) after soaking with **EK3–18** (light blue, 9H2Z) or in an alternate apo form (yellow, 3 N4 U), (B) in complex with ADP (salmon, 4 N57) and (C) in complex with kanamycin A (green, 4DFB). Ligands are shown as sticks.

confirmed the presence of plasmid-borne *aph(2″)-IVa* while we did not detect other *aph* genes. We challenged this strain with **EK3**-based inhibitors and assessed the effect on the minimal inhibitory concentrations (MICs) of a variety of aminoglycosides (Table 1). The strain shows high-level of resistance to aminoglycosides with a MIC between 1 and 4 mg/mL. In the presence of **EK3**-based compounds, we observed no effect on bacterial growth in the absence of aminoglycoside, but a dose-dependent decrease of the aminoglycoside MIC values. At 256 μg/mL, the highest concentration of inhibitor tested, we measured a 5–6 $\log_2$ decrease of the MIC values for the four aminoglycosides tested. In line with kinetic inhibition data and for almost all the concentrations tested, **EK3–18** displayed a greater efficiency than **EK3** and **EK3–17**, reducing the MIC values by one or two further $\log_2$. In these conditions, susceptibility of the *Enterococcus* isolate to gentamicin and tobramycin has been restored according to Eucast clinical breakpoints guidelines.[45] Gentamicin is the most used aminoglycoside in clinics, often prescribed for its efficient synergism effect with β-lactams. As a control, we evaluated the ability of **EK3** compound to inhibit the APH(2″)-IVa-mediated deactivation of gentamicin *in vitro*. We found that the compound displayed a similar level and mode of inhibition than previously determined with kanamycin A (Figure S3). This suggests that **EK3** compounds are effective to prevent aminoglycoside deactivation of all substrates modified by the APH(2″)-IVa enzyme.

Table 1. Effect of EK3-based inhibitors on the bacterial aminoglycoside susceptibility. Comparison of antibiotic susceptibility of an *Enterococcus casseliflavus* isolate expressing the *aph(2″)-IVa* gene in the absence or presence of **EK3**, **EK3–17** or **EK3–18**. Inhibitor concentrations of 0 (No inh.), 64, 128 and 256 and MIC values are expressed as μg/mL. The (+) symbol indicates standard bacterial growth in the absence of antibiotic but in the presence of **EK3** compounds at indicated concentrations. For **EK3**-based compounds, 256 μg/mL corresponds to 0.78–0.82 mM, concentrations smaller than the maximal dose showing no cytotoxic effect (Figure 7).

	MIC values (μg/mL)									
	No inh.	EK3			EK3-17			EK3-18		
	0	64	128	256	64	128	256	64	128	256
Kanamycin A	2048	512	128	64	1024	256	128	256	64	32
Gentamicin	4096	1024	512	256	2048	1024	512	512	256	64
Tobramycin	4096	1024	512	128	2048	512	256	512	128	64
Sisomicin	1024	1024	512	64	512	256	64	128	64	32
No antibiotic	+	+	+	+	+	+	+	+	+	+

EK3-Based Inhibitors are not Cytotoxic to HeLa Human Cells

With the aim to use **EK3**-based inhibitors, or a pharmacologically optimized compound, as an aminoglycoside combined therapeutic, we evaluated their toxicity to human cells using the Cell Proliferation Kit II (XTT). This kit is widely-used to quantitatively assess drug toxicity *in cellulo*. As shown in Figure 7, the viability of HeLa cells was not affected, even at 1 mM of inhibitors.

Conclusions

Aminoglycosides are among the most commonly used antimicrobial agents in clinical practice, due to their ability to treat a variety of acute bacterial infections. However, the efficacy of these antibiotics is constantly threatened by the production of

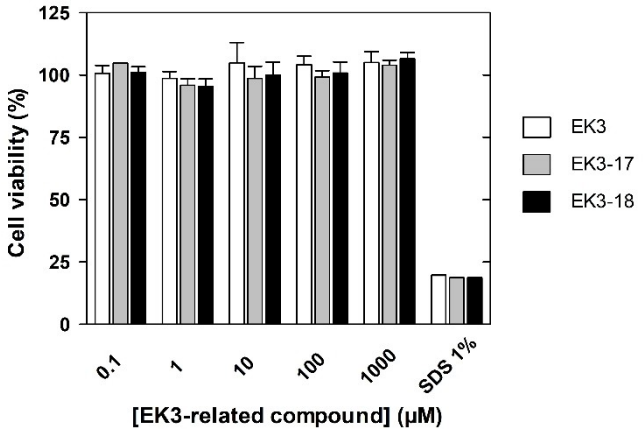

Figure 7. Cytotoxicity assays of EK3 and related compounds. Viability of HeLa cells in the presence of indicated concentrations of **EK3** (white bars), **EK3–17** (grey bars) or **EK3–18** (black bars) was measured using the an XTT-based colorimetric assay. SDS at 1% was used as a negative control. Results are expressed as mean versus cell viability obtained without compound but at the same DMSO concentration (1%) ± standard deviation for three independent replicates. For SDS, the error bars are not visible due to low dispersion of the data (SD ranging from 0.14–0.27% cell viability).

AMEs, the most frequently reported aminoglycosides resistance mechanism. These enzymes therefore represent promising targets for the design of reverting agents. Over the last few decades, a number of studies have focused on the development of inhibitors capable of restoring aminoglycoside activity by inhibiting AMEs, and in particular APHs.

The family of APHs, also called aminoglycoside kinases, includes a variety of structurally related enzymes. In particular, they contain a nucleotide-binding domain which presents a high degree of structural similarity, also shared with eukaryotic protein kinases (ePKs).[14] Thus, several known ATP-competitive inhibitors of protein kinases such as sulfonamide, flavonoids and wortannin, have been tested against the APH(3′)-IIIa and APH(2″)-Ia enzymes, demonstrating a good level of inhibition.[19,46] Likewise, crystal structures of APH(3′)-IIIa and APH(9)-Ia have been determined in complex with CKI-7, an inhibitor of the casein kinase 1 from the isoquinoline sulfonamide family, which, similarly to ePKs, was found to bind to the nucleotide-binding pocket.[47,48] The interaction of different ePK inhibitors with APH(3′)-Ia from *E. coli* has also been investigated.[21] In this study, crystal structures of the enzyme were determined in complex with a number of kinase inhibitors, including the ePK pyrazolopyrimidine inhibitors PP1 and PP2 that were found in the nucleotide-binding site of APH(3′)-Ia, acting as ATP-competitive inhibitors. The same group previously screened 80 kinase inhibitors against 12 APHs belonging to six different APH subfamilies, including the APH(3″)-IIIa and the APH(2″)-IVa.[20] They found that most of them were also APH inhibitors acting competitively toward the nucleotide. Among them, the flavonoid natural product quercetin displayed activity against all tested APHs and a crystal structure of APH(2″)-IVa in complex with quercetin, revealed a binding mode common to that of nucleotides. The degree of inhibition of APHs by quercetin (K_i~25 μM) was similar to that determined here for **EK3**. However, most of the APH inhibitors described so far are competitive molecules which lack specificity for APHs as they also impact important ePK functions, limiting their use *in vivo*. A recent study performed pharmacophore modeling and docking to identify inhibitors of APH(3′)-IIIa from *Enterococcus faecalis*. These molecules were filtered to select potential competitive inhibitors binding to the ATP pocket, so further work will be necessary to determine their effect on ePKs.[49]

Here, we used computational methods combining molecular dynamics and virtual screening to select a subset of candidate molecules targeting an allosteric protein pocket adjacent to, but distinct from, the nucleotide-binding site. This approach exploits an intrinsic property of most if not all enzymes which is their conformational flexibility, critical for their function. By binding to allosteric sites, modulators may indeed (i) slow down the transition towards an active state (perturbing enzyme dynamics by trapping the protein in a particular conformational state), (ii) perturb enzyme oligomerization, or (iii) prevent the formation of a crucial intermediate conformational state.[50,51] While competitive orthosteric inhibitors target active sites, the most conserved regions among diverse families of enzymes, allosteric modulators bind to sites which present a higher degree of variability. This approach has the benefit of avoiding targeting the ATP-binding site that is conserved between APHs and ePKs.

From a small chemical library of 12,000 compounds and from testing only 14 molecules *in vitro*, we successfully identified an non-competitive inhibitor of APH(2″)-IVa from *E. casseliflavus*. Using a similar strategy targeting a different APH cavity located behind the aminoglycoside binding site, we previously identified, from a pool of only 17 molecules tested *in vitro*, two inhibitors of APH(3′)-IIIa from *E. faecalis* and APH(2″)-IVa from *E. casseliflavus*.[22] Among them, the molecule called NL6 was confirmed to be a non-competitive inhibitor yet the level of inhibition against both enzymes was 8-fold lower (K_i~80 μM) than measured here for **EK3–18**. Altogether, these results highlight the high success rate of this strategy compared to conventional *in vitro* screenings of large libraries.[51–53] To our knowledge, the **EK3** inhibitors identified here constitute the most potent allosteric inhibitors of APH(2″)-IVa described so far. Moreover, our allosteric inhibitors do not appear to be toxic to HeLa cells in culture, suggesting that they are more specific than previous ePK inhibitors tested on APHs.

Given the intrinsic tolerance of enterococci to aminoglycosides, it is not surprising that the bacterial isolate tested here presents high MICs (1,024–4,096 μg/mL). According to the European Committee on Antimicrobial Susceptibility Testing (EUCAST),[54] enterococci isolates with gentamicin MIC $\leq$ 128 μg/mL are considered as susceptible. When used at 256 μg/mL, **EK3–18**, our most efficient inhibitor reduces the MIC below this threshold. For other aminoglycoside antibiotics, especially sisomicin, the sensitivity is restored even in the presence of 64 μg/mL inhibitor. However, this concentration remains high and more optimization of this compound is necessary to further improve its *in vitro* efficacy. To this end, additional structural work providing molecular insight into the inhibitor binding mode would not only aid development of a more active

inhibitor of APH(2″)-IVa, but also assist the design of broader antibacterial compounds targeting other APHs.

Experimental Section

Molecular Dynamics Simulations and Docking

Three APH structures were used for molecular dynamics simulations and virtual screening: APH(3′)-IIIa (PDB 1J7L), APH(2″)-IIa (PDB 4DCA formerly 3R70) and APH(2″)-IVa (PDB 4DBX). Each ligand-free protein was immersed in a water box (10 Å edge around the solute) and neutralized by addition of salt ions (Na^+/Cl^-). The potential energy of each system was minimized with 50,000 steps of conjugate gradient using the CHARMM36 all-atom force field topology and parameters[55] and the program NAMD (v2.11).[56] After a gradual heating from 0–310 K, a short equilibration (2 ns) was performed in explicit water (TIP3P water model) to remove steric clashes with CMAP protein backbone energy correction terms and periodic boundary conditions. The Lennard-Jones potential was smoothly truncated from 10–12 Å and the PME (Particle Mesh Ewald) algorithm was used to calculate long-range electrostatics with a grid spacing of 1 Å. After equilibration, a production run of 200 ns was carried out in the isobaric-isothermal ensemble. This simulation time was selected as sufficient for sampling and detecting small cavities as checked by a longer simulation (additional 200 ns performed for APH(2″)-IVa to ensure a more in-depth sampling). Temperature (310 K) and pressure (1 atm) were kept constant by Langevin dynamics and Nosé-Hoover Langevin piston coupled to the water bath. From the production trajectory 2,000 conformations (snapshots) were extracted and used for pocket detection using Fpocket or MDpocket.[57–59]

Virtual screening was performed using GOLD program (Genetic Optimization for Ligand Docking, v5.2) from CCDC Software Limited[38] on the three APH ensemble. The nucleotide (ADP) was kept for 1J7L, 3R70 and introduced in 4DBX by superimposition to 3R70 structure (an energy minimization step was performed prior docking). Preliminary screening indicated that docking scores were much lower for 4DBX structure than other APHs. Thus, a more open conformation of the protein was generated by computing the normal modes using the Elastic Network Model from ElNemo[60] and this conformation was used for the screening. Three amino acid side chains were defined as freely flexible during docking for all APHs (using the rotamers library of GOLD) for K44, E60 and D208 (numbering refers to 1J7L) in order to increase ligand accessibility. The target cavity (previously identified by MDpocket) was defined by setting a spherical area around the cavity center coordinates and a radius of 10 Å. A chemical library encompassing 12,000 molecules was collected from the ZINC database[37] and filtered to fulfill drug-like properties (Lipinski's rule of 5) and higher polarity. The genetic algorithm (50 runs) allowed the search of best docking orientations (poses) for each chemical entity and further ranked by the GoldScore scoring function by using the clustering method (complete linkage) from the RMSD matrix of docking solutions. The final ranking of best hits was determined according to their docking scores and commercial availabilities. Visual Molecular Dynamics (VMD 1.9.2)[56] was used to analyze the simulations and extract the 2,000 conformations from the simulation trajectory.

Chemicals

All aminoglycosides, ATP and other chemicals were purchased from Merck, previously Sigma-Aldrich, at the highest purity grade. Small molecule compounds, referred to as EK molecules, were ordered from Molport (http://www.molport.com), dissolved in DMSO at 100 mM final concentration before being aliquoted and stored at −20 °C. ATP in the text refers to MgATP containing equimolar concentrations of nucleotide and $MgCl_2$. Stock solutions of aminoglycosides and ATP at 5 and 10 mM respectively were prepared in 50 mM Tris-HCl pH 7.5, 40 mM KCl and 1 mM $MgCl_2$ and stored at −20 °C.

Kinetic Measurements

The N-terminally 6His-tagged recombinant APHs were produced in *E. coli* BL21 cells according to the procedure already published.[35] Typical yields were 70, 80 and 50 mg/L of overnight culture for the APH(2″)-IIa, APH(2″)-IVa and APH(3′)-IIIa, respectively. Proteins were stored at −20 °C in a buffer containing 50 mM Hepes pH 7.5, 1 mM $MgCl_2$ and 50 % glycerol. All kinetic measurements were performed in a buffer containing 50 mM Tris-HCl pH 7.5, 40 mM KCl and 1 mM free $MgCl_2$.

To rapidly screen the effect of EK compounds on the three APH enzymes, we utilized the protein kinase (PK) and lactate dehydrogenase (LDH) enzymatic coupled assay as already described.[24] In brief, free ADP production was coupled to NADH consumption, monitored at 340 nm, in the presence of 0.5 μM APH, 500 μM EK compound, 350 μM ATP, 100 μM kanamycin A with an excess of PK, LDH and their respective substrates as described earlier.[61] Reactions were carried out in 96-well plates at 25 °C. The steady-state rate constants, k_{ss}, were calculated from the slope of the linear phase of the reaction using GraFit (Version 7.0.3, Erithacus Software Limited). Results were normalized to controls containing no EK compound but identical DMSO concentration.

The mode of inhibition of **EK3** and structurally-related compounds was determined by the quench-flow method and HPLC analysis as described earlier.[35] By this technique, concentrations of total ADP, i.e. enzyme-bound plus free ADP are obtained. Time courses were fitted globally (altogether) with GraFit software using the four different inhibition modes: competitive, non-competitive, mixed and uncompetitive, and transformed as Lineweaver-Burk representations. Initial concentrations of ATP, kanamycin A and EK compound are indicated in the figure legend. In all assays, DMSO final concentration was matching the highest concentration of EK compound.

Crystallization, Data Collection and Structure Determination

The APH(2″)-IVa at 6 mg/mL was mixed at a 1:1 ratio with a crystallization solution composed of 10 % PEG3350 and 50 mM ammonium citrate pH 7.5 in a 2 μL final volume. Crystallogenesis was performed at 18 °C in EasyXtal 15-well plates by the hanging-drop vapor diffusion method over a reservoir of 500 μL. Microseeding using crystals obtained in the same conditions was used to promote growth of larger crystals. After crystal formation, 0.1 μL of **EK3–18** at 100 mM in DMSO was added to the drop and left for 5 min. Longer soaking times resulted in crystal degradation and poor X-ray diffraction. Crystals were then flash frozen in liquid nitrogen in nylon loops. Data were collected on beamline ID30 A-1 (MASSIF-1) at ESRF, indexed with XDS-Autoprocess[62] and scaled with Aimless.[63] Structure was solved by molecular replacement with Phaser,[64] using a previous solved structure of the protein (5C4L)[35] as model after removal of ligand and water molecules. The structure was subsequently built and refined using Coot[65] and Refmac[66] and validated with RAMPAGE[67] and PROCHECK.[68]

Cell Viability Assay

Approximately 7,500 HeLa cells were plated in flat-bottom 96-well plates in a final volume of 100 μL. After 24 h of incubation at 37 °C and 5 % CO_2, cells were treated with indicated concentrations of EK compound, respecting a final DMSO concentration of 1 %. Positive and negative controls were performed by omitting small compound and adding either identical DMSO concentration or 1 % SDS, respectively. Cell viability was assessed after two days of treatment using the Cell Proliferation Kit II protocol (XTT, Roche). Measurements were carried out by reading absorbance at 470 nm with a reference wavelength of 660 nm. The results of three independent repetitions were averaged and normalized to the mean of vehicle control wells containing no EK compound but identical DMSO concentration.

Bacterial DNA Extraction and Identification of *aph* Genes by PCR

Plasmid DNA was isolated using the NucleoSpin™ plasmid kit from Macherey-Nagel while genomic DNA was obtained as follows. Two to three colonies grew on LB agar were lysed in 25 μL of 0.25 % SDS, 0.05 M NaOH and boiled for 15 min as described earlier.[9] Cell lysates were then diluted with 200 μL of sterile water and 5 μL of this mixture were used for the PCR reaction.

DNA amplification experiments were performed in a final volume of 25 μL containing 10 ng or 5 μL of plasmid and genomic DNA, respectively, 200 μM dNTP, 1X PCR buffer, 2.5 U Taq DNA polymerase (New England Biolabs) and 0.5 μM of each primer (Sigma) for the detection of three aminoglycoside resistance *aph* genes listed in Table 2. After an initial denaturation step of 3 min at 94 °C, 35 cycles of 40 s at 94 °C, 40 s at 56 °C and 40 s at 72 °C were carried out, before a final extension stage of 2 min at 72 °C. Positive controls were included using cloning vectors containing each *aph* gene from enterococci. PCR products were visualized on 1.5 % agarose gels.

Evaluation of Antibiotic Bacterial Susceptibility

Aminoglycoside bacterial susceptibility was evaluated by the broth microdilution method in the absence or presence of EK compounds, measuring the minimal inhibitory concentration (MIC) which corresponds to the lowest concentration of aminoglycoside resulting in complete inhibition of bacterial growth. Overnight precultures of an *Enterococcus casseliflavus* isolate expressing the *aph(2'')-IVa* gene (Pasteur Institute Collection, CIP 111947, ATCC 700668) were realized by inoculation of 3 mL of Mueller-Hinton (MH) broth with bacteria conserved as 50 % glycerol stocks at −80 °C. After 16 h of growth under shaking at 37 °C, bacteria were diluted 100-fold in 3 mL of fresh MH broth and incubated for an additional 2 h to get exponential growth phase cultures.

Measurements were performed in 96-well plates (Microtest Tissue Culture plates, Falcon) filled with 100 μL/well MH media containing 10^6 CFU/mL, supplemented or not with different concentrations of aminoglycoside antibiotic and EK compounds. Specifically, we added 100 μL of MH to the wells of column 1 (sterility control, negative control), 50 μL of MH to the wells of columns 3–11 and 75 μL to column 12 (growth control, positive control). We added 100 μL of aminoglycoside solution at 8,192 μg/mL to the wells of column 2 and proceed to a two-fold dilution series until column 11 from which 50 μL were thrown away. 25 μL of solutions containing 4 % DMSO (1 % final) and different concentrations of EK compounds were added to the wells as follow: 1st line 0 μg/mL, 2nd line 256 μg/mL (64 μg/mL final), 3rd line 512 μg/mL (128 μg/mL final) and 4th line 1,024 μg/mL (512 μg/mL final). Finally, 25 μL of inoculum at 0.004 OD_{600} (0.001 final OD_{600}) were added.

MICs were assessed after 24 h growth at 37 °C. Antibiotic breakpoints were determined according to recommendations of the European Committee on Antimicrobial Susceptibility Testing (EUCAST).[54]

Table 2. List of primers used for detection of *aph* genes. The melting temperature (Tm) for each primer is indicated.

Gene	Sequence (5′–3′)	Tm (°C)	Size (bp)
aph(2'')-Ila	CTTGGACGCTGAGATATATGAGCAC	62.0	867
	GTTTGTAGCAATTCAGAAACACCCTT	61.6	
aph(2'')-Iva	GTGGTTTTTACAGGAATGCCATC	60.4	641
	CCCTCTTCATACCAATCCATATAACC	60.7	
aph(3')-IIIa	GGCTAAAATGAGAATATCACCGG	59.7	523
	CTTTAAAAAATCATACAGCTCGCG	60.1	

Supporting Information Summary

Table S1. Docking scores and relative APH activities of **EK** compounds.

Table S2. Docking scores of **EK3** analogues in APH(2'')-IVa·ADP structure.

Table S3. X-ray data and refinement statistics.

Figure S1. Determination of the mode of inhibition of APH(2'')-IVa by **EK3**.

Figure S2. Determination of the mode of inhibition of APH(2'')-IVa by **EK3–17** or **EK3–18**.

Figure S3. Determination of the mode of inhibition of APH(2'')-IVa by **EK3** using gentamicin as aminoglycoside substrate.

Movie S1. Molecular dynamics trajectories of APHs and associated selected cavity.

Movie S2. Conformational change observed after soaking of APH(2'')-IVa crystal with **EK3–18**.

Acknowledgements

This work was supported by ANR SIAM (ANR-19-AMRB-0001), CNRS, INSERM and University of Montpellier. This work benefited from access to the X-ray facilities of the Integrated Biophysics and Structural Biology Platform (PIBBS) of the CBS. PIBBS is a GIS-IBISA platform and belongs to the French Infrastructure for Integrated Structural Biology (FRISBI), supported by the National Research Agency (ANR-10-INBS-

0005).We thank Dr. Muriel Gelin (CBS) for her help in collecting crystallographic data and Dr. Pierre Germain (CBS) for his help to perform cytotoxicity assays. We thank Dr. Olivier Chesneau (Institut Pasteur) for the *aph(2'')-IVa* expressing *Enterococcus* strain. We would like to thank Drs. Nicholas P. Greene (Univ. of Cambridge, UK), Cédric Orelle and Jean-Michel Jault (IBCP) for their careful proofreading of the manuscript. We are grateful to Dr. Yinshan Yang (CBS) for helpful discussions.

Conflict of Interests

The authors declare no conflict of interest.

Data Availability Statement

Coordinates and structure factors have been deposited in the PDB under the accession code 9H2Z.

Keywords: Allostery · Antibiotic resistance · Inhibitors · Molecular docking · Virtual screening

[1] K. M. Krause, A. W. Serio, T. R. Kane, L. E. Connolly, *Cold Spring Harb. Perspect. Med.* **2016**, *6*, a027029.
[2] L. P. Kotra, J. Haddad, S. Mobashery, *Antimicrob. Agents Chemother.* **2000**, *44*, 3249–3256.
[3] A. P. Carter, W. M. Clemons, D. E. Brodersen, R. J. Morgan-Warren, B. T. Wimberly, V. Ramakrishnan, *Nature* **2000**, *407*, 340–348.
[4] B. D. Davis, *Microbiol. Rev.* **1987**, *51*, 341–350.
[5] G. G. Zhanel, D. J. Hoban, G. K. Harding, *DICP* **1991**, *25*, 153–163.
[6] G. M. Eliopoulos, C. T. Eliopoulos, *Clin. Microbiol. Rev.* **1988**, *1*, 139–156.
[7] P. Cottagnoud, M. Cottagnoud, M. G. Täuber, *Antimicrob. Agents Chemother.* **2003**, *47*, 144–147.
[8] M. S. Ramirez, M. E. Tolmasky, *Drug Resist. Updat.* **2010**, *13*, 151–171.
[9] S. B. Vakulenko, S. Mobashery, *Clin. Microbiol. Rev.* **2003**, *16*, 430–450.
[10] B. Llano-Sotelo, E. F. Azucena, L. P. Kotra, S. Mobashery, C. S. Chow, *Chem. Biol.* **2002**, *9*, 455–463.
[11] E.-J. Yoon, C. Grillot-Courvalin, P. Courvalin, *J. Antibiot. (Tokyo)* **2017**, *70*, 400–403.
[12] E. Azucena, I. Grapsas, S. Mobashery, *J. Am. Chem. Soc.* **1997**, *119*, 2317–2318.
[13] C. A. Smith, M. Toth, T. M. Weiss, H. Frase, S. B. Vakulenko, *Acta Crystallogr. D Biol. Crystallogr.* **2014**, *70*, 2754–2764.
[14] W. C. Hon, G. A. McKay, P. R. Thompson, R. M. Sweet, D. S. Yang, G. D. Wright, A. M. Berghuis, *Cell* **1997**, *89*, 887–895.
[15] J. Roestamadji, I. Grapsas, S. Mobashery, *J. Am. Chem. Soc.* **1995**, *117*, 11060–11069.
[16] A. Bastida, A. Hidalgo, J. L. Chiara, M. Torrado, F. Corzana, J. M. Pérez-Cañadillas, P. Groves, E. Garcia-Junceda, C. Gonzalez, J. Jimenez-Barbero, J. L. Asensio, *J. Am. Chem. Soc.* **2006**, *128*, 100–116.
[17] K. T. Welch, K. G. Virga, N. A. Whittemore, C. Özen, E. Wright, C. L. Brown, R. E. Lee, E. H. Serpersu, *Bioorg. Med. Chem.* **2005**, *13*, 6252–6263.
[18] J. B. Aggen, E. S. Armstrong, A. A. Goldblum, P. Dozzo, M. S. Linsell, M. J. Gliedt, D. J. Hildebrandt, L. A. Feeney, A. Kubo, R. D. Matias, S. Lopez, M. Gomez, K. B. Wlasichuk, R. Diokno, G. H. Miller, H. E. Moser, *Antimicrob. Agents Chemother.* **2010**, *54*, 4636–4642.
[19] D. M. Daigle, G. A. McKay, G. D. Wright, *J. Biol. Chem.* **1997**, *272*, 24755–24758.
[20] T. Shakya, P. J. Stogios, N. Waglechner, E. Evdokimova, L. Ejim, J. E. Blanchard, A. G. McArthur, A. Savchenko, G. D. Wright, *Chem. Biol.* **2011**, *18*, 1591–1601.
[21] P. J. Stogios, P. Spanogiannopoulos, E. Evdokimova, O. Egorova, T. Shakya, N. Todorovic, A. Capretta, G. D. Wright, A. Savchenko, *Biochem. J.* **2013**, *454*, 191–200.
[22] N. Leban, E. Kaplan, L. Chaloin, S. Godreuil, C. Lionne, *Biochim. Biophys. Acta, Gen. Subj.* **2017**, *1861*, 3464–3473.
[23] A. Kohl, P. Amstutz, P. Parizek, H. K. Binz, C. Briand, G. Capitani, P. Forrer, A. Plückthun, M. G. Grütter, *Structure* **2005**, *13*, 1131–1141.
[24] G. A. McKay, P. R. Thompson, G. D. Wright, *Biochemistry* **1994**, *33*, 6936–6944.
[25] D. H. Fong, A. M. Berghuis, *EMBO J.* **2002**, *21*, 2323–2331.
[26] M. Toth, J. Zajicek, C. Kim, J. W. Chow, C. Smith, S. Mobashery, S. Vakulenko, *Biochemistry* **2007**, *46*, 5570–5578.
[27] J. W. Chow, V. Kak, I. You, S. J. Kao, J. Petrin, D. B. Clewell, S. A. Lerner, G. H. Miller, K. J. Shaw, *Antimicrob. Agents Chemother.* **2001**, *45*, 2691–2694.
[28] S. F. Tsai, M. J. Zervos, D. B. Clewell, S. M. Donabedian, D. F. Sahm, J. W. Chow, *Antimicrob. Agents Chemother.* **1998**, *42*, 1229–1232.
[29] D. L. Burk, W. C. Hon, A. K. Leung, A. M. Berghuis, *Biochemistry* **2001**, *40*, 8756–8764.
[30] P. G. Young, R. Walanj, V. Lakshmi, L. J. Byrnes, P. Metcalf, E. N. Baker, S. B. Vakulenko, C. A. Smith, *J. Bacteriol.* **2009**, *191*, 4133–4143.
[31] K. Shi, A. M. Berghuis, *J. Biol. Chem.* **2012**, *287*, 13094–13102.
[32] C. Kim, J. Haddad, S. B. Vakulenko, S. O. Meroueh, Y. Wu, H. Yan, S. Mobashery, *Biochemistry* **2004**, *43*, 2373–2383.
[33] C. Kim, J. Y. Cha, H. Yan, S. B. Vakulenko, S. Mobashery, *J. Biol. Chem.* **2006**, *281*, 6964–6969.
[34] P. Lallemand, N. Leban, S. Kunzelmann, L. Chaloin, E. H. Serpersu, M. R. Webb, T. Barman, C. Lionne, *FEBS Lett.* **2012**, *586*, 4223–4227.
[35] E. Kaplan, J. F. Guichou, L. Chaloin, S. Kunzelmann, N. Leban, E. H. Serpersu, C. Lionne, *Biochim. Biophys. Acta – Gen. Subj.* **2016**, DOI 10.1016/j.bbagen.2016.01.016.
[36] J. J. Irwin, B. K. Shoichet, *J. Chem. Inf. Model.* **2005**, *45*, 177–182.
[37] J. J. Irwin, T. Sterling, M. M. Mysinger, E. S. Bolstad, R. G. Coleman, **2012**, DOI 10.1021/ci3001277.
[38] G. Jones, P. Willett, R. C. Glen, A. R. Leach, R. Taylor, *J. Mol. Biol.* **1997**, *267*, 727–748.
[39] M. L. Verdonk, J. C. Cole, M. J. Hartshorn, C. W. Murray, R. D. Taylor, *Proteins* **2003**, *52*, 609–623.
[40] C. Liao, Y. Wang, X. Tan, L. Sun, S. Liu, *Sci. Rep.* **2015**, *5*, 10754.
[41] T. E. Barman, S. R. W. Bellamy, H. Gutfreund, S. E. Halford, C. Lionne, *Cell. Mol. Life Sci.* **2006**, DOI 10.1007/s00018-006-6243-z.
[42] M. Toth, H. Frase, N. T. Antunes, C. A. Smith, S. B. Vakulenko, *Protein Sci.* **2010**, DOI 10.1002/pro.437.
[43] D. Bajusz, A. Rácz, K. Héberger, *J. Cheminf.* **2015**, *7*, 20.
[44] M. Toth, H. Frase, N. T. Antunes, C. A. Smith, S. B. Vakulenko, *Protein Sci.* **2010**, *19*, 1565–1576.
[45] The European Committee on Antimicrobial Susceptibility Testing. *Breakpoint Tables for Interpretation of MICs and Zone Diameters. Version 10.0.* **2020** .
[46] D. D. Boehr, W. S. Lane, G. D. Wright, *Chem. Biol.* **2001**, *8*, 791–800.
[47] D. H. Fong, A. M. Berghuis, *Acta Crystallogr. D Biol. Crystallogr.* **2004**, *60*, 1897–1899.
[48] D. H. Fong, B. Xiong, J. Hwang, A. M. Berghuis, *PLoS ONE* **2011**, *6*, e19589.
[49] L. A. Velez, S. D. Arteaga, **2024**, DOI 10.1101/2024.12.23.630124.
[50] J. Monod, J. P. Changeux, F. Jacob, *J. Mol. Biol.* **1963**, *6*, 306–329.
[51] B. S. DeDecker, *Chem. Biol.* **2000**, *7*, R103–107.
[52] G. M. Lee, C. S. Craik, *Science* **2009**, *324*, 213–215.
[53] P. Wu, M. H. Clausen, T. E. Nielsen, *Pharmacol. Ther.* **2015**, *156*, 59–68.
[54] European Committee for Antimicrobial Susceptibility Testing (EUCAST) of the European Society of Clinical Microbiology and Infectious Diseases (ESCMID), *Clin. Microbiol. Infect.* **2003**, *9*, ix–xv.
[55] R. B. Best, X. Zhu, J. Shim, P. E. M. Lopes, J. Mittal, M. Feig, A. D. Mackerell, *J. Chem. Theory Comput.* **2012**, *8*, 3257–3273.
[56] J. C. Phillips, R. Braun, W. Wang, J. Gumbart, E. Tajkhorshid, E. Villa, C. Chipot, R. D. Skeel, L. Kalé, K. Schulten, *J. Comput. Chem.* **2005**, *26*, 1781–1802.
[57] V. Le Guilloux, P. Schmidtke, P. Tuffery, *BMC Bioinf.* **2009**, *10*, 168.
[58] P. Schmidtke, V. Le Guilloux, J. Maupetit, P. Tufféry, *Nucleic Acids Res.* **2010**, *38*, W582–589.
[59] P. Schmidtke, A. Bidon-Chanal, F. J. Luque, X. Barril, *Bioinformatics* **2011**, *27*, 3276–3285.
[60] K. Suhre, Y.-H. Sanejouand, *Nucleic Acids Res.* **2004**, *32*, W610–614.
[61] N. Leban, E. Kaplan, L. Chaloin, S. Godreuil, C. Lionne, *Biochim. Biophys. Acta Gen. Subj.* **2017**, *1861*, 3464–3473.
[62] C. Vonrhein, C. Flensburg, P. Keller, A. Sharff, O. Smart, W. Paciorek, T. Womack, G. Bricogne, *Acta Crystallogr. D Biol. Crystallogr.* **2011**, *67*, 293–302.
[63] P. R. Evans, G. N. Murshudov, *Acta Crystallogr. D Biol. Crystallogr.* **2013**, *69*, 1204.

[64] A. J. McCoy, R. W. Grosse-Kunstleve, P. D. Adams, M. D. Winn, L. C. Storoni, R. J. Read, *J. Appl. Crystallogr.* **2007**, *40*, 658–674.
[65] P. Emsley, B. Lohkamp, W. G. Scott, K. Cowtan, *Acta Crystallogr. D Biol. Crystallogr.* **2010**, *66*, 486–501.
[66] G. N. Murshudov, P. Skubák, A. A. Lebedev, N. S. Pannu, R. A. Steiner, R. A. Nicholls, M. D. Winn, F. Long, A. A. Vagin, *Acta Crystallogr. D Biol. Crystallogr.* **2011**, *67*, 355–367.
[67] S. C. Lovell, I. W. Davis, W. B. Arendall III, P. I. W. de Bakker, J. M. Word, M. G. Prisant, J. S. Richardson, D. C. Richardson, *Proteins Struct. Funct. Bioinf.* **2003**, *50*, 437–450.
[68] R. A. Laskowski, M. W. MacArthur, D. S. Moss, J. M. Thornton, *J. Appl. Cryst.* **1993**, *26*, 283–291.

Manuscript received: October 24, 2024
Revised manuscript received: January 9, 2025
Accepted manuscript online: January 13, 2025
Version of record online: ■■, ■■

RESEARCH ARTICLE

Molecular dynamics simulations and in silico screening were used to identify non-competitive inhibitors of APH, the enzymes that confer resistance to aminoglycoside antibiotics. A hit molecule showed activity against APH(2″)-IVa. Allosteric inhibition by the hit molecule and a two-fold more potent analogue was confirmed by enzymatic measurements. Both inhibitors restored sensitivity to various aminoglycosides in a resistant strain of enterococci.

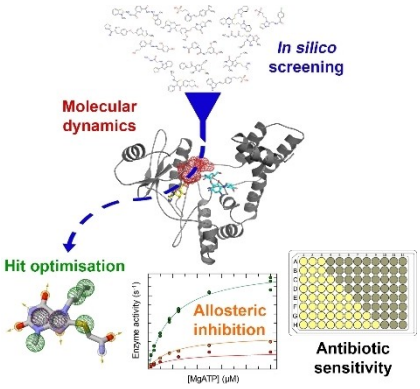

E. Kaplan, L. Chaloin, J.-F. Guichou, K. Berrou, R. Rahimova, G. Labesse, C. Lionne**

1 – 12

APH Inhibitors that Reverse Aminoglycoside Resistance in *Enterococcus casseliflavus*